

NJC

Accepted Manuscript



This is an *Accepted Manuscript*, which has been through the Royal Society of Chemistry peer review process and has been accepted for publication.

Accepted Manuscripts are published online shortly after acceptance, before technical editing, formatting and proof reading. Using this free service, authors can make their results available to the community, in citable form, before we publish the edited article. We will replace this *Accepted Manuscript* with the edited and formatted *Advance Article* as soon as it is available.

You can find more information about *Accepted Manuscripts* in the [Information for Authors](#).

Please note that technical editing may introduce minor changes to the text and/or graphics, which may alter content. The journal's standard [Terms & Conditions](#) and the [Ethical guidelines](#) still apply. In no event shall the Royal Society of Chemistry be held responsible for any errors or omissions in this *Accepted Manuscript* or any consequences arising from the use of any information it contains.

Effect of synergic cooperation on optical and photoelectrochemical properties of CeO₂-MnO composite thin films[†]

Cite this: DOI: 10.1039/x0xx00000x

Received 00th January 2012,
Accepted 00th January 2012

DOI: 10.1039/x0xx00000x

www.rsc.org/

Muhammad Adil Mansoor,^{ab} Muhammad Mazhar,^{*a} Mehdi Ebadi,^c Huang Nay Ming,^b Mohd Asri Mat Teridi,^d Lo Kong Mun.^a

CeO₂-MnO composite thin films have been deposited on fluorine doped tin oxide (FTO) coated glass substrates by aerosol assisted chemical vapor deposition (AACVD) using a 1:1 mixture of cerium complex, [Ce(OCOCF₃)₄][[(CH₃)₂NHCH₂CH₂OH]⁺ (**1**), and acetato manganese(II). X-ray diffraction (XRD), Raman spectroscopy and profilometer were used to investigate phase purity, stoichiometry and thickness of the films. EDX results confirmed Ce to Mn ratio of 1:9 in the deposited composite thin film. The FEG-SEM analysis illustrated that the morphology of the fabricated films was influenced by the deposition temperature and hence optoelectronic properties. UV-vis studies of the composite thin film fabricated from methanol solution at 475 °C demonstrate a direct band gap of 2.5 eV. From the current-voltage characteristics it is evident that the CeO₂-MnO composite semiconductor electrode exhibits n-type behavior and the photocurrent was strongly dependent on the deposition temperature. The CeO₂-MnO photoanode deposited at 475 °C for 45 min from 0.023 M solution of (**1**) and acetatomanganese(II) in methanol gave a maximum photocurrent density of 265 μA cm⁻² at 0.65 V vs. Ag/AgCl/3M KCl using 0.5 M NaOH electrolyte.

Keywords: CeO₂-MnO composite oxide, thin film, band gap, synergic effect, photoelectrochemical.

1. Introduction

Over the past years, cerium oxide and its composite materials have come under scrutiny as catalysts, structural and electronic promoters in heterogeneous catalysis.¹⁻⁴ When associated with transition metal oxides, ceria films have received great interest because of their high transparency in the visible and near-IR region and electrooptical performance.^{5,6} Manganese oxides are also considered important in many technological applications. Mn₂O₃ is known to be an active catalyst for removing carbon monoxide and nitrogen oxide from waste gases⁷ while MnO, MnO₂ and Mn₂O₃ have been used as photoanode⁸ and to catalyse water oxidation in a photooxidant system.⁹⁻¹³ Among these oxides of manganese, MnO due its high chemical and structural stability and low cost has been studied widely as an anode material for lithium ion batteries in the form of its

composites with other materials such as Fe₂O₃, ZnO, graphite, reduced graphene, carbon nano tubes etc.¹⁴⁻¹⁷ Keeping in view the chemical stability of MnO in electrochemical cell, we decided to use it as a photoanode for photoelectrochemical water splitting while reducing its band gap by addition of some dopant or composite formation with some other suitable metal oxide. Studies have revealed that within a composite metal oxide system charge-transfer transition between conduction bands or the valence bands of the semiconducting oxide takes place thereby causing a decrease in band gap energy.^{18, 19} The coupling of two semiconductors²⁰ or the deposition of noble metal nanoparticles²¹ results in improved interfacial charge transfer and thereby minimizing charge recombination.²² Therefore, we have chosen CeO₂ semiconductor metal oxide to engineer the band gap of MnO and to enhance its photoelectrochemical efficiency. CeO₂ is already reported for

its importance in band gap engineering and photoactivity in the form of composites with other materials such as ZnO, ZrO₂, Bi₂O₃, MnO₂, TiO₂ etc.²³⁻²⁶

Given the structural and compositional complexity of oxide materials, it is not surprising that synthesis can affect the functional properties in a dramatic manner. This is particularly manifested in thin films where non-equilibrium deposition conditions can lead to large variations in film properties. The origins of these differences are related not only to the microstructural differences that come about due to synthesis, but also to the variation in oxygen and in some cases cation content. Although a variety of techniques^{8, 9, 13, 27-30} have been implemented to prepare ceramic materials thin films, nevertheless, we chose aerosol assisted chemical vapour deposition (AACVD) technique because of its several advantages such as excellent film uniformity, high deposition rates, conformal coverage on complex geometries, controllability of film microstructures, low cost and scalability. Herein we report the synthesis of CeO₂-MnO composite thin film using oxygen rich precursor (**1**) for CeO₂ and acetato manganese(II), as both have matching solubility properties to act as dual source for the deposition of CeO₂-MnO composite thin films applying AACVD at relatively low temperatures of 450, 475 and 500 °C. The deposited films were characterised by XRD, FT-IR, Raman, SEM, EDX and UV-Vis spectrophotometry for their stoichiometry, morphology, thickness and optical band gap. A further scope of these thin film electrodes towards harvesting sunlight for the generation of photoelectric current was investigated and reported here.

2. Experimental

2.1. Material and Methods

All manipulations were carried out under an inert atmosphere of dry argon, using Schlenk tubes and glove box techniques. The solvents and reagents were purchased from Aldrich. The solvents were rigorously dried on sodium benzoate and distilled immediately before use. The melting point was determined in a capillary tube using an electrothermal melting point apparatus; model MP.D Mitamura Riken Kogyo (Japan). The microanalyses were performed using Leco CHNS 932. FT-IR spectra were recorded on a single reflectance ATR instrument (4000–400 cm⁻¹, resolution 4 cm⁻¹). The NMR was recorded by JEOL DELTA2 NMR Spectrometer at field strength of 400 MHz using DMSO-d₆ as a solvent. The controlled thermal analysis was investigated using a METTLER TOLEDO TGA/SDTA 851e Thermogravimetric Analyzer with a computer interface. The thermal measurements were carried out in an alumina crucible under an atmosphere of flowing nitrogen gas (20 cm³ min⁻¹) with a heating rate of 20 °C min⁻¹. The surface morphology of thin films was studied using a field-emission gun scanning electron microscope (FEG-SEM, FEI Quanta 400) coupled with Energy Dispersive X-ray spectrometer EDX (INCA Energy 200 (Oxford Inst.)), at an accelerating voltage of 10 kV, and a working distance of 9 mm. The phase purity was examined by using X-ray powder diffraction (XRD) on a D8 Advance X-Ray Diffractometer-Bruker AXS using Cu-K α radiation ($\lambda = 1.542 \text{ \AA}$), at a voltage of 40 kV and current of 40 mA at ambient temperature. Raman spectroscopy was carried out using a RENISHAW, IN VIA, WIRE 3.4 (with 514 nm Ar laser) Raman Spectrophotometer. The spectrum was recorded in the range from 100–1000 cm⁻¹. The thickness of the films was determined by using

profilometer KLA Tencore P-6 surface profiler. The average thickness was found to be 509, 515 and 498 nm of the films deposited at 450, 475 and 500 °C respectively, using methanol solvent. The optical absorption spectrum of these films was recorded on a Lambda 35 Perkin-Elmer UV-Vis spectrophotometer in the wavelength range of 330–830 nm. The photo-electrochemical response of fabricated CeO₂-MnO layers was studied by a three-electrode configuration cell using an external potential bias source (Autolab/PGSTAT 240). *J-V* characteristics were performed through the linear sweep photovoltammetry (LSPV) technique (potential window range: -0.2 to +0.7 V, and scan rate 10 mV s⁻¹) while the reference, counter and working electrodes were Ag/AgCl (saturated KCl), platinum sheet and fabricated electrodes, respectively. PEC test for solar activated decomposition of water was carried out once the electrodes were inserted in the quartz window cell contained with 0.5 M NaOH in the dark and light (150 W Xe lamp: 100 mW cm⁻²) conditions.

2.2. Synthesis of [Ce(OCOCH₃)₄][(CH₃)₂NHCH₂CH₂OH]⁺ (**1**)

A mixture of acetylacetonato cerium(III) hydrate (0.5 g, ~1.14 mmol) and trifluoroacetic acid (0.35 mL, 4.57 mmol) in 20 mL of THF in a Schlenk tube under argon atmosphere was stirred for 8 h. The reaction mixture was then evacuated to powder and re-dissolved in 3 mL of toluene followed by the addition of *N,N*-dimethyl-2-aminoethanol (0.114 mL, 1.14 mmol) under vacuum. The complex (**1**) was isolated from toluene solution at -10 °C in 75% yield. Mp: 125 °C. Micro analysis: % calculated (found) for [Ce(OCOCH₃)₄][(CH₃)₂NHCH₂CH₂OH]⁺ C, 21.11 (20.93), H, 1.77 (1.66), N, 2.05 (1.92). FT-IR/cm⁻¹: 3345(b), 2791(w), 1738(s), 1643(w), 1439(m), 1427(s), 1391(w), 1187(s), 1133(s), 1077(s), 1057(m), 922(s), 829(m), 718(s), 604(m), 521(m). ¹H NMR $\delta = 3.63$ ppm [t, OCH₂], $\delta = 3.38$ ppm [s, H], 3.07 ppm [t, NCH₃] and $\delta = 2.71$ ppm [s, 2 x CH₂]. ¹⁹F-NMR $\delta = -73.90$ ppm [s, 3F, CF₃]. TGA: 247–330 °C 68.5 and 330–705 °C 74.9% weight loss. Crystals suitable for single crystal X-ray diffraction study were obtained from toluene. Single crystal XRD measurement was performed on a CCD diffractometer (Bruker Smart APEX II) with graphite monochromatized MoK α radiation, $\lambda_{M\alpha} = 0.71073 \text{ \AA}$. Data reduction was carried out using the SAINT program. Semi empirical absorption corrections were applied on equivalent reflections using SADABS. The structure solution and refinements were performed using SHELXS-2013 and SHELXL-2013 program packages.

2.3. Deposition of thin films by AACVD

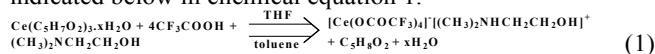
The films were deposited on commercially available FTO glass substrate of resistivity 8 Ω /sq using self-designed aerosol assisted chemical vapor deposition assembly.³¹ The FTO substrates purchased from Sigma Aldrich were cut to the dimension of 25.4 × 12.7 × 2.2 mm (L × W × D) and cleaned prior to use by ultrasonically washing with distilled water, acetone, and then ethyl alcohol. Finally, they were washed with distilled water, stored in ethanol, and dried in air. Substrate slides of the dimension of 25.2 mm × 12.7 mm were placed inside the reactor tube and then heated up to the deposition temperature for 10 min to stabilize the temperature before carrying out the deposition. The aerosols of the precursor solution were formed by keeping the round bottom flask in a water bath above the piezoelectric modulator of an ultrasonic humidifier. The generated aerosol droplets of the precursor were transferred into the hot wall zone of the reactor by argon

gas. The exhaust from the reactor was vented directly into the extraction system of a fume cupboard. At the end of the deposition, the aerosol line was closed and only carrier gas passed over the substrate. The substrate was allowed to cool to 30 °C before it was taken out from the reactor. In a typical deposition experiment, a homogeneous mixture of acetatomanganese(II) (0.10 g, 0.58 mmol) and $[\text{Ce}(\text{OCOCF}_3)_4]^-$ $[(\text{CH}_3)_2\text{NHCH}_2\text{CH}_2\text{OH}]^+$ (**1**) (0.37 g, 0.58 mmol) was dissolved in 25 mL methanol solution and utilized for the fabrication of CeO_2 -MnO thin films for 45 min. The carrier gas at a flow rate of 120 mL/min was controlled by a LIX linear flow meter. The deposited thin films are light yellow coloured, transparent, uniform, robust, and stable towards atmospheric conditions and adhere strongly on FTO substrate as verified by the “scotch tape test”.³²

3. Results and discussion

3.1. An insight into the complex (1)

The acetylacetonato cerium(III) hydrated dissolves in trifluoroacetic acid with the complete replacement of three acetylacetonato ligands bound to cerium by four trifluoroacetato ligands leading to the formation of an anionic specie $[\text{Ce}(\text{OCOCF}_3)_4]^-$. The charge is balanced by protonation of $(\text{CH}_3)_2\text{NCH}_2\text{CH}_2\text{OH}$ to form N,N -dimethylethanolammonium ion $[(\text{CH}_3)_2\text{NHCH}_2\text{CH}_2\text{OH}]^+$ as indicated below in chemical equation 1.



The stoichiometry of the complex has been ascertained by microanalysis, FT-IR, ¹H-NMR, thermogravimetry and single crystal X-ray diffraction analysis. The FT-IR spectrum of complex (**1**) shows the presence of characteristic vibrations of functional groups attached to the cerium atoms in (**1**). A broad absorption band at 3365 cm⁻¹ indicated the presence of OH group. The absorption frequencies of $[(\text{CH}_3)_2\text{NHCH}_2\text{CH}_2\text{OH}]^+$ at 1077 cm⁻¹ varied from those reported for free $(\text{CH}_3)_2\text{NCH}_2\text{CH}_2\text{OH}$ at 1040 cm⁻¹.³³ The symmetric and asymmetric ν(C=O) vibrations of trifluoroacetato ligand have been identified at 1643 and 1419 cm⁻¹ respectively. The difference of 224 cm⁻¹ between asymmetric and symmetric ν(C=O) vibrations indicates the bidentate nature of the carboxylate groups of trifluoroacetato ligands that are bonded to different cerium centres.³⁴ Similarly, the peak at 1187 cm⁻¹ confirms the presence of C-F bonds in complex (**1**). The absorptions at the low frequency of 521 cm⁻¹ is due to ν(M–O) stretching vibrations. (Figure S1).³⁵ The ¹H-NMR shows four signals at δ = 3.63 ppm [t, OCH₂], δ = 3.38 ppm [s, H], 3.07 ppm [t, NCH₃] and δ = 2.71 ppm [s, 2 x CH₂] due to $[(\text{CH}_3)_2\text{NHCH}_2\text{CH}_2\text{OH}]^+$ (Figure S2). The ¹⁹F-NMR shows a singlet at δ = -73.90 ppm [s, 3F, CF₃] indicating the presence of trifluoroacetato ligand in complex (**1**) (Figure S3).³⁶

The ORTEP diagram of the polymeric Ce(III) carboxylate is depicted in figure 1. Summary of the crystallographic data, selected bond distances and angles are given in Tables S1 and S2, respectively. Four trifluoroacetate moieties are involved in the coordination through the exodentate carboxylate oxygen atoms with the Ce(III) metal centers and generate the “paddle-wheel” type coordination in the polymeric chain. The resulting Ce(III) metal centers were rendered negatively charge which were countered balanced by the presence of the N,N -dimethylethanol ammonium cations. The ionic salt was stabilized by the presence of hydrogen bonding interactions between the hydroxyl group of the N,N -dimethylethanol

ammonium cations and the carboxylate oxygen atom of one of the trifluoroacetate $[\text{O9-H}\dots\text{O5}^i = 2.776(4) \text{ \AA}$, symmetry operator $i: x, y, z+1$]. As shown in figure 2, the molecular cationic fragments are also linked to each other by means of a cyclic R²₂(10) type of N-H...O hydrogen bond motifs $[\text{N1-H}\dots\text{O9}^{ii} = 2.786(5) \text{ \AA}$, symmetry operator $ii: -x+1, -y+1, -z+1$]. Each Ce(III) metal center in the polymeric chain has a square antiprismatic geometry with the square base provided by carboxylate oxygen atoms. The Ce --- Ce distances $[4.457 - 4.575 \text{ \AA}]$ in the polymeric chain are much longer than the sum of covalent for Ce (~4.08 Å). The average Ce---O distances of the carboxylic oxygen around the Ce(III) metal center is in the range of 2.452(3) – 2.571(3) Å.

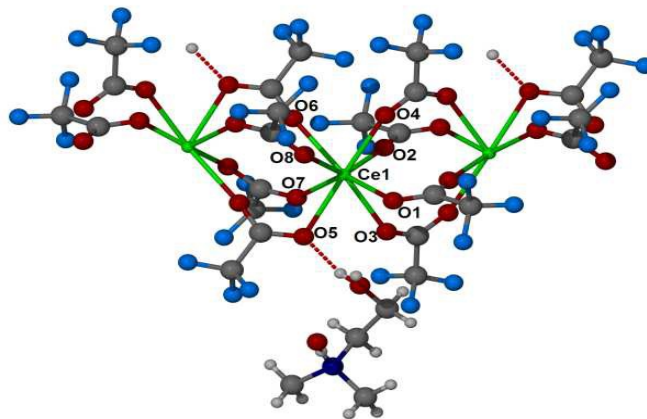


Figure 1. Molecular plot for $[\text{Ce}(\text{OCOCF}_3)_4]^-$ $[(\text{CH}_3)_2\text{NHCH}_2\text{CH}_2\text{OH}]^+$ with atom labelling scheme.

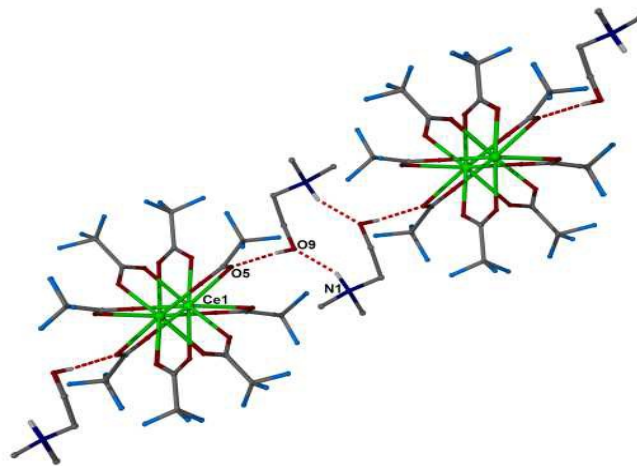


Figure 2. Polymeric chain of $[\text{Ce}(\text{OCOCF}_3)_4]^-$ $[(\text{CH}_3)_2\text{NHCH}_2\text{CH}_2\text{OH}]^+$ viewed down the a axis, depicting the presence of intermolecular OH..O and NH..O hydrogen bondings.

3.2. Pyrolysis of complex (1)

The pyrolysis behaviour of (**1**) has been studied by thermogravimetric (TGA) and differential thermogravimetric (DTG)

analyses implemented under flowing nitrogen ambient at a flow rate of 25 cm³/min with heating rate of 20 °C/min (Figure 3). The DTG indicates that the complex (1) decomposes in two steps with the first major degradation in the temperature range of 247–330 °C with weight loss of 68.5%. The second pyrolysis step is slow and occurs in a wide temperature range of 330–705 °C with weight loss of 74.9%. The residual mass of 25.1% of original mass of the precursor (1) indicates complete decomposition of the complex to CeO₂ as indicated in the chemical equation 2. These observations suggest potential of the complex (1) for its implementation for the fabrication of Ce-Mn composite oxide thin films.

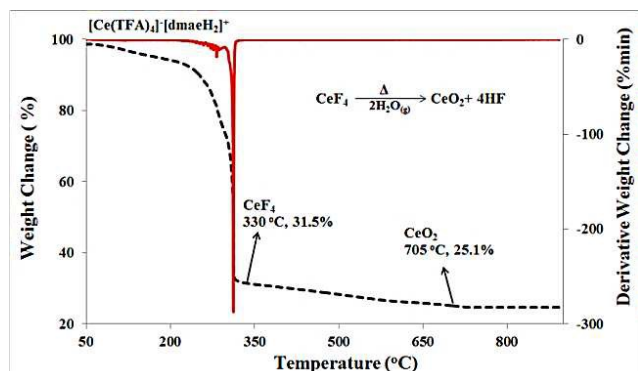
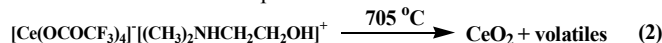


Figure 3. TGA (black dashed line) and DTG (red solid line) plot of $[\text{Ce}(\text{OCOCF}_3)_4][(\text{CH}_3)_2\text{NHCH}_2\text{CH}_2\text{OH}]^+$ (1) under nitrogen flow rate of 25 cm³ min⁻¹ and heating rate of 20 °C min⁻¹.

Further GCMS studies (ESI Table S3) of the volatile matter obtained from pyrolysis of complex (1) suggest that the peaks appearing at *m/z* value of 43, 71 and 85 are due to the major fragmented species CO₂, CF₃OH, and CHF₃, respectively that are obtained from the decomposition of trifluoroacetato ligand attached to cerium. This observation is in line with the previous similar studies.^{37, 38} The fragments having peaks at *m/z* value of 17, 28, 45, 61, 75 and 90 are assigned to H₂O, C₂H₄, (CH₃)₂NH, (CH₃)₂NOH, CH₃NH(CH₂)₂OH and [(CH₃)₂NHCH₂CH₂OH]⁺ species respectively that are expected to be evolved from the breakdown of [(CH₃)₂NHCH₂CH₂OH]⁺ cation.

3.3. Crystallinity and chemical structure of thin films

To identify the chemical nature and crystallinity, X-ray diffraction of CeO₂–MnO (1:9) composite thin films fabricated at 450, 475 and 500 °C on FTO coated glass substrate was recorded and is presented in Figure 4. The relative peak intensities and the position of the diffraction peaks of the CeO₂–MnO composite thin film diffractograms are in good agreement with ICDD card No [98-005-5284] and [98-000-9864] for CeO₂ and MnO respectively. Stick pattern matching with standard cards are available in supplementary materials as Figure S4.

Both CeO₂ and MnO exhibit cubic crystal systems with space group *Fm-3m* and cell parameters of *a* = 5.5130 and 4.4460 Å respectively. In the XRD spectrum (Figure 4), the peaks at 2θ values of 28.1°, 32.6°, 46.2° and 54.8° correspond respectively to (111), (002), (022) and (113) lattice reflection planes of a cubic CeO₂ phase, whereas peaks at 2θ values of 35.1°, 40.6° and 58.8° correspond respectively to (111), (002) and (022) lattice reflection planes of cubic MnO phase. A small peak at 46.2° for CeO₂ seems to be suppressed. We speculate that the suppression and broadening in CeO₂ peaks are due to low

concentration and small grain size.³⁹ This phenomenon is further supported by broad and weak Raman scattering at 462 cm⁻¹.

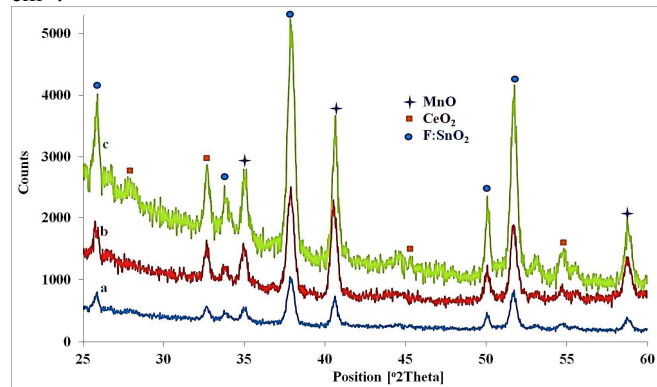


Figure 4. XRD of the as-grown CeO₂–MnO composite thin films fabricated on FTO glass at deposition temperatures of (a) 450, (b) 475 and (c) 500 °C.

Raman active modes of synthesized CeO₂–MnO composite thin films were identified by comparison with the literature values. Raman spectrum (Figure 5) of CeO₂–MnO fabricated at 475 °C, shows that the three fundamental scattering modes at 645, 364 and 308 cm⁻¹ are due to MnO,⁴⁰ while the characteristic scattering mode of CeO₂ falls at 462 cm⁻¹.⁴¹ There are several reports dealing with relationship between Raman scattering modes and grain size of nanostructured materials.^{39, 42} These reports indicate that the Raman line broadening and decrease in intensity has inverse relation with grain size. It is also reported that intensity of Raman scattering is directly dependent on concentration of crystalline material.^{43, 44} Thus we consider that the low concentration and smaller grain size may be the key factors that result in peak broadening and reduction in peak intensity of CeO₂ at 462 cm⁻¹.

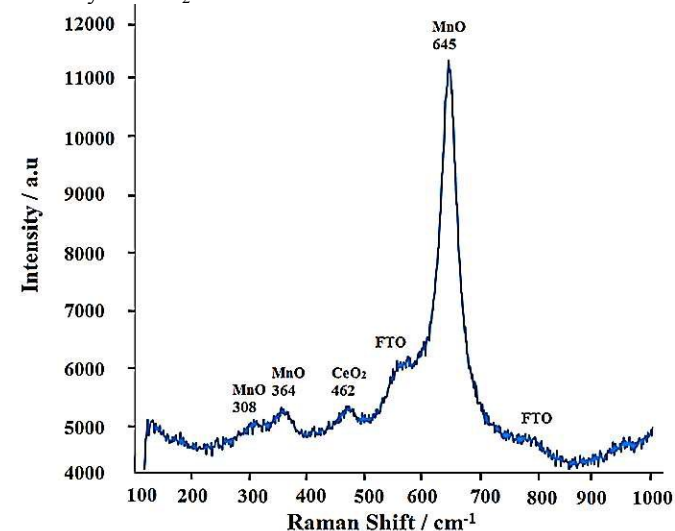


Figure 5. Raman spectrum of CeO₂–MnO photoanode synthesised from a solution of (1) and acetatomanganese(II) in methanol at 475 °C by AACVD.

To investigate the effect of FTO substrate on XRD and Raman spectra of the thin films, CeO₂–MnO composite oxide powder with metallic ratio of 1:9 was prepared under conditions similar to thin film deposition (ESI Figure S5 and S6). The Raman spectrum and the XRD pattern of the powdered composite

agree very well with the patterns obtained from the thin films of CeO₂-MnO composite. This observation eliminates any possibility of chemical interference of FTO glass substrate during thin film fabrication.

3.4. Surface morphology

The FE-SEM images of the films deposited at 450, 475 and 500 °C for 45 min from methanol solution of the precursor are presented respectively in Figure 6(a-c). The results illustrate that the film morphology is significantly influenced by the deposition temperature. The film deposited at 450 °C (Figure 6a) shows agglomerates with compact structure with no definite shape. On the other hand, the film deposited at 475 °C (Figure 6b) show agglomerates with spherical particles embedded within the lumps, where the size of agglomerated lumps is in range of 0.3-0.7 μm. The film fabricated at 500 °C shows the agglomerated particles have joined together to form bigger spherical lumps in size range of 1.3-1.9 μm. The films tailored at 500 °C display more voids as compared to the films deposited at 450 and 475 °C (Figure 6c). The formation of thin films with different morphology and structure with respect to change in deposition temperature can be explained on the basis of homogeneous and heterogeneous nucleation at the time of deposition as reported in the literature.^{45, 46} There are possibilities to attain four types of morphologies depending on type of nucleation reaction that may take place during AACVD and is summarized as follow.

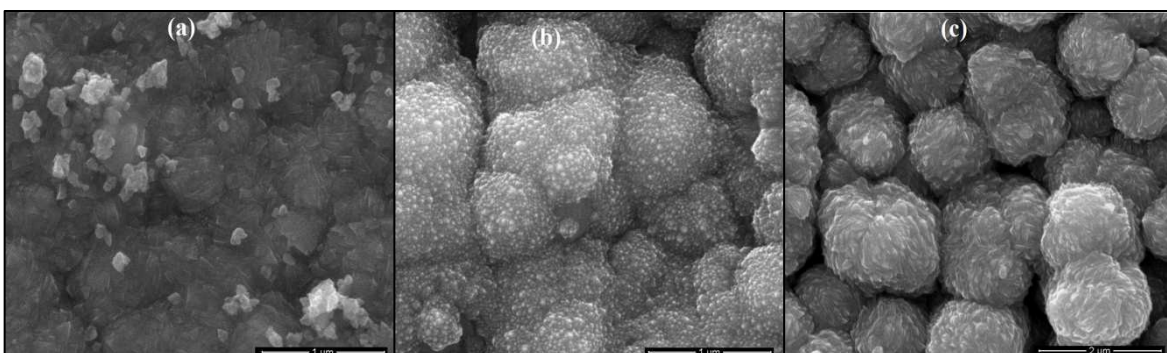


Figure 6. FE-SEM images of CeO₂-MnO composite thin films deposited on FTO substrate at (a) 450, (b) 475 and (c) 500 °C for 45 min.

3.5. Optical band gap

The UV-Vis spectrum of the composite CeO₂-MnO thin films fabricated at 450, 475 and 500 °C recorded in region of 350-850 nm is shown in Figure 7 (a-c). It is apparent that the film absorbs maximum in near UV region with a prominent steep of absorbance from 450-750 nm in visible range of light. The absorbance of light is directly related to the thickness of film which is evident in the present work that the film fabricated at 475 °C with average thickness of 515 nm shows maximum absorbance and least in the case of film fabricated at 500 °C with average thickness of 498 nm. The direct optical band gaps of the thin films deposited at 450, 475 and 500 °C were determined by Tauc's plot as shown in inset of figure 7a-c.⁴⁸⁻⁵¹

The reported band gap is 2.8 and 3.69 eV for CeO₂⁵² and MnO respectively.⁵³ However, we found band gap edge at 2.42, 2.5 and 2.4 eV for the CeO₂-MnO composite thin films fabricated at 450, 475 and 500 °C respectively. A decrease in band gap energy values

The homogeneous reaction that takes place at low temperature may lead to films with hierarchical structure while homogeneous reaction taking place at high deposition temperature may result in porous agglomerated structure.

The homogeneous and heterogeneous reactions occurring simultaneously under low temperature regime will lead to compact structure with some voids whereas the homogeneous and heterogeneous reactions occurring simultaneously at high temperature conditions may produce agglomerates with more voids.

Present studies reveal that the homogeneous and heterogeneous reactions occurring simultaneously at 450 and 475 °C are resulting in the formation of compact structures with less voids whereas films fabricated at 500 °C have more voids and porous structures which is in relevance to the earlier work reported on Bi₂S₃.⁴⁵ It is worth to mention that choice of solvent is also one of the key factors in controlling homogeneous or heterogeneous reactions. In present studies we have used methanol which is already reported elsewhere³⁶ for both type of reactions simultaneously leading to compact structure.

The EDX spectrum (Figure S7) of the thin films deposited at 475 °C indicates cerium to manganese ratio of 1:9. The molar concentration of both the precursors was maintained at 1:1, but only 10% of cerium contents were found to be present in the deposit. The lower cerium contents that were found in the deposit are explained by the fact that cerium complex (I) is ionic in nature and high in molecular weight, that reduces its throughput in the aerosol as compared acetatomanganese(II).⁴⁷

of CeO₂-MnO composite thin film was observed as compared to the band gap energies of individual CeO₂ and MnO. This decrease may be explained on the basis of synergic cooperation between the two components of the CeO₂ and MnO composite material. It is most probable that the electrons jump from conduction band of CeO₂ to the conduction band of MnO that reduces recombination of electrons at the same time increasing the life time of e⁻ and h⁺ (Figure 9). Similar studies on CeO₂ composites with CuO, TiO₂, Fe₂O₃, CuBi₂O₄ etc. have been reported^{48, 54-56} which reflect the similar synergistic effect imparted by CeO₂ in attaining low band gap with better absorbance in visible region of the light.

3.6. Photoelectrochemical properties

Figure 8 shows the current density–voltage (*J*-*V*) plot for the CeO₂-MnO thin films fabricated under similar conditions at 450, 475 and 500 °C. The CeO₂-MnO thin film electrodes exhibit an anodic photocurrent which gradually increases with

the increase of anodic bias. It is shown in Figure 8 that the photocurrent density is highly dependent on deposition temperature. As we raise deposition temperature from 450 to 475 °C, photocurrent density increases, with further increase of the deposition temperature to 500 °C, the photocurrent of CeO₂-MnO photoelectrodes decreases significantly. We believe that at low deposition temperature of 450 °C, the deposited particles are dislocated without adaptation of any definite shape that reduces uniformity. These dislocations and non-uniform structure may act as the recombination centres for the photogenerated electron-hole pairs. At the same time compactness of the particles causes to reduce electrode-electrolyte interface surface area leading to a poor PEC performance as shown in Figure 6a. At higher deposition temperature of 500 °C particles agglomerate to bigger spherical lumps and produce voids between the particles, that lead to loss of electron in voids and channels resulting in decline of photocurrent density as displayed in Figure 6c).⁵⁷

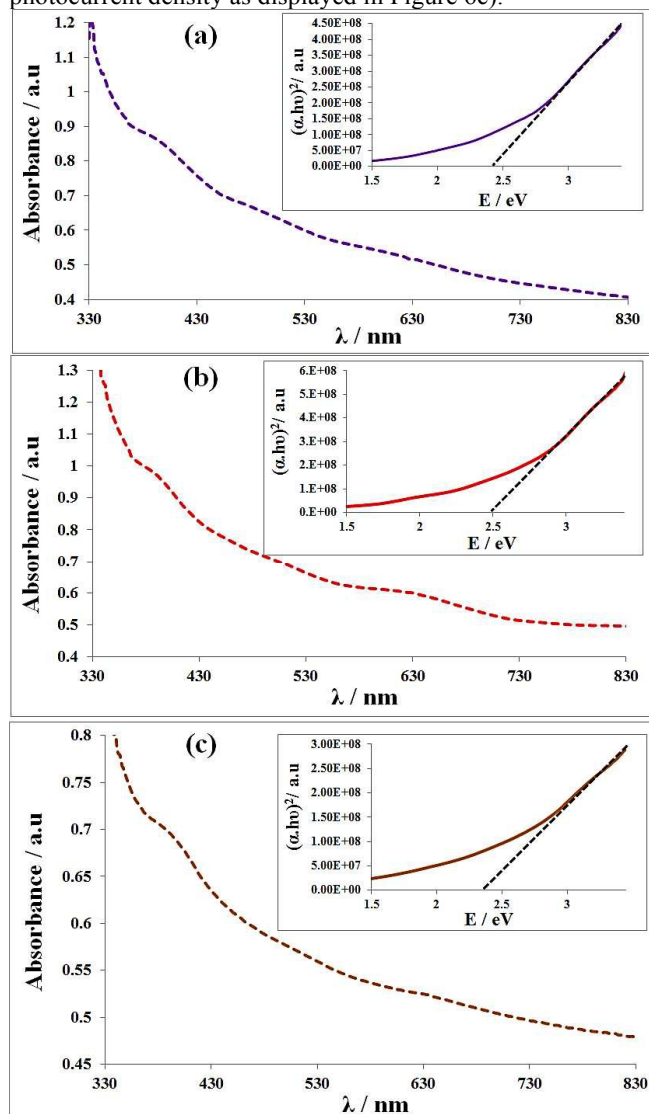


Figure 7. UV-Vis spectra of absorbance as a function of wavelength and inset Tauc plots ($(\alpha h\nu)^2$ Vs E/eV) of CeO₂-MnO composite thin films deposited at (a) 450, (b) 475 and (c) 500 °C from a solution of **(1)** and acetatomanganese(II) in methanol.

The CeO₂-MnO composite thin film fabricated at 475 °C is relatively uniform and contains less voids and channels that produces maximum photocurrent density of 265 $\mu A/cm^2$ at applied voltage of 0.65 V using 0.5 M NaOH (pH = 13) as electrolyte and Ag/AgCl as standard electrode. MnO has been widely studied as anodic materials for lithium ion batteries and somewhere as coating material for Si-electrodes⁵⁸ but it is hard to find its literature regarding photoelectrochemical water splitting. Among the other oxides of manganese, MnO₂ is widely studied for its photoelectrochemical properties, which could produce photocurrent density of 20 $\mu A/cm^2$ under similar basic conditions of pH = 13.

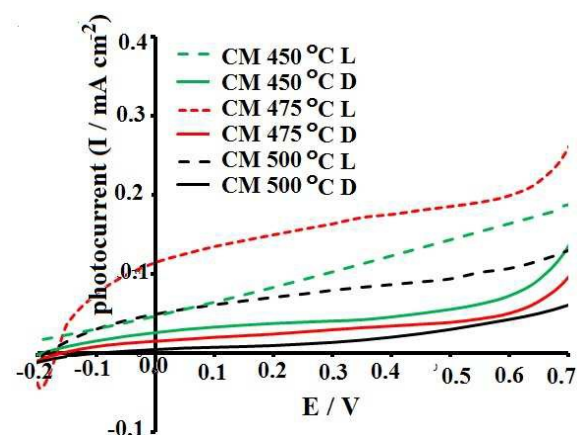


Figure 8. Dependence of photocurrent density under illumination (L) and dark (D) conditions on different deposition temperatures for the fabrication of CeO₂-MnO photoanode.

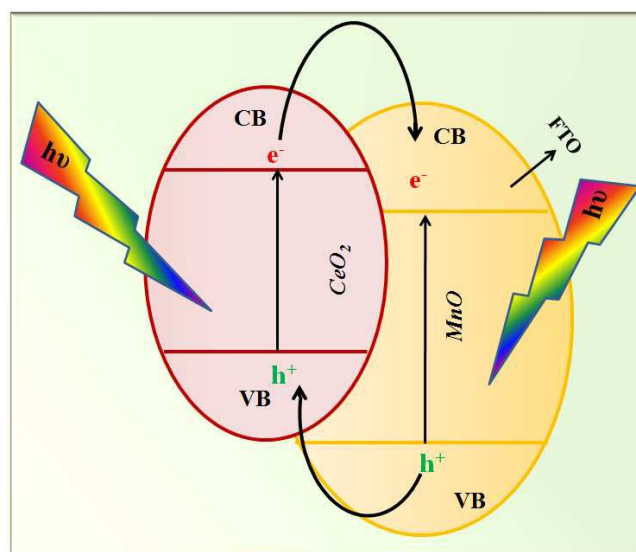


Figure 9. The plausible hole-trapping and electron transfer mechanisms for CeO₂-MnO composite thin films in sunlight exposure.

It is most probable that the photo-excitation of electrons from the valance band of CeO₂ into its conduction band and subsequently their transfer to the low energy conduction band of MnO followed by their transfer to external circuit *via* FTO, reduces e^-h^+ recombination as shown in Figure 9. The hole trapping process is facilitated in the mixed semiconductor system which increases the photogeneration efficiency. Therefore, the photogeneration efficiency of the electron-hole

pair in the CeO₂-MnO composite semiconductor system is enhanced as compared to the pure CeO₂ or MnO. The resulting trapped holes at the surface of photoanode interact with water for its photooxidation to O₂ and H⁺ ions. The H⁺ ions are transported through the electrolyte towards the counter electrode where they react with photogenerated electrons to produce hydrogen.^{4, 59}

Further improvement in photocurrent can be brought about by improving thin film quality, by optimization of film thickness, surface roughness, crystallinity, structure and geometry.

4. Conclusions

Thin films of CeO₂-MnO (1:9) composite in the size range of 0.3-0.7 μm are grown onto FTO-coated glass substrate by AACVD utilizing a newly synthesized complex, [Ce(OCOFCF₃)₄][(CH₃)₂NHCH₂CH₂OH]⁺ (**1**) and acetatomanganese(II) as dual source precursors. The composite formation not only lowers the band gap energy but also suppresses the possibility of e⁻-h⁺ recombination to enhance photoactivity. A band gap of 2.5 eV and a maximum photocurrent density of 265 μA/cm² at 0.65 V vs. Ag/AgCl/3MKCl have been obtained for photoelectrodes grown from methanol solution at 475 °C.

Acknowledgements

MM, HNM and MAMT acknowledge High-Impact Research Grant No. UM.C/625/1/HIR/242, UMRG Grant No. UM.TNC2/RC/261/1/1/RP007-13AET, UM.C/625/1/HIR/MOHE/SC/21 and ICONIC-2013-005 for funding this research.

Notes and references

^aDepartment of Chemistry, Faculty of Science, University of Malaya, Kuala Lumpur 50603, Malaysia. Phone: +60379674269 Email: mazhar42pk@yahoo.com.

^bLow Dimensional Materials Research Centre, Department of Physics, Faculty of Science, University of Malaya, 50603 Kuala Lumpur, Malaysia.

^cDepartment of Chemistry, Faculty of Sciences, Islamic Azad University-Gorgan Branch, Gorgan, Iran.

^dSolar Energy Research Institute, University Kebangsaan Malaysia, 43600 Bangi, Selangor, Malaysia

†CCDC 1421004 contains the supplementary crystallographic data for compound (**1**). The data can be obtained free of charge via <http://www.ccdc.cam.ac.uk/conts/retrieving.html>, or from the Cambridge Crystallographic Data Centre, 12 Union Road, Cambridge CB2 1EZ, UK; fax: (+44) 1223 336 033; or e-mail: deposit@ccdc.cam.ac.uk

Electronic Supplementary Information (ESI) available: [Supporting figures for FTIR, NMR, GC-MS, XRD and EDX are available in ESI]. See DOI: 10.1039/b000000x/

1. F. C. Larachi, J. Pierre, A. Adnot and A. Bernis, *App. Surf. Sci.*, 2002, **195**, 236.
2. T. Ghoshal, P. G. Fleming, J. D. Holmes and M. A. Morris, *J. Mater. Chem.*, 2012, **22**, 22949.
3. I. M. I. Ismail, M. Aslam, T. Almeelbi, S. Chandrasekaran and A. Hameed, *RSC Adv.*, 2014, **4**, 16043.

4. M. Aslam, I. M. I. Ismail, S. Chandrasekaran, T. Almeelbi and A. Hameed, *RSC Adv.*, 2014, **4**, 49347.
5. M. A. Sainz, A. Durán and J. M. Fernández Navarro, *J. Non-Cryst. Solids*, 1990, **121**, 315.
6. N. Özer, *Sol. Energy Mater. Sol. Cells*, 2001, **68**, 391.
7. M. Baldi, V. S. Escibano, J. M. G. Amores, F. Milella and G. Busca, *App. Catal. B: Environmental*, 1998, **17**, L175.
8. I. Zaharieva, P. Chernev, M. Risch, K. Klingan, M. Kohlhoff, A. Fischer and H. Dau, *Energy Environ. Sci.*, 2012, **5**, 7081.
9. D. M. Robinson, Y. B. Go, M. Mui, G. Gardner, Z. Zhang, D. Mastrogianni, E. Garfunkel, J. Li, M. Greenblatt and G. C. Dismukes, *J. Am. Chem. Soc.*, 2013, **135**, 3494.
10. V. B. R. Boppana and F. Jiao, *Chem. Commun.*, 2011, **47**, 8973.
11. M. M. Najafpour, T. Ehrenberg, M. Wiechen and P. Kurz, *Angew. Chem. Int. Ed.*, 2010, **49**, 2233.
12. F. Jiao and H. Frei, *Chem. Commun.*, 2010, **46**, 2920.
13. Y. Gorlin and T. F. Jaramillo, *J. Am. Chem. Soc.*, 2010, **132**, 13612.
14. M. M. Thackeray, C. S. Johnson, J. T. Vaughey, N. Li and S. A. Hackney, *J. Mater. Chem.*, 2005, **15**, 2257.
15. M. S. Song, S. Nam, W. I. Cho and C. Lee, *Chem. Chem. Phys.*, 2015, **17**, 23496.
16. B.-K. Zou, Y.-Y. Zhang, J.-Y. Wang, X. Liang, X.-H. Ma and C.-H. Chen, *Electrochim. Acta*, 2015, **167**, 25.
17. S. Zhang, L. Zhu, H. Song, X. Chen and J. Zhou, *Nano Energy*, 2014, **10**, 172.
18. Y. Lu, Y. Lin, T. Xie, S. Shi, H. Fan and D. Wang, *Nanoscale*, 2012, **4**, 6393.
19. Y. Yang, Y. Li, L. Zhu, H. He, L. Hu, J. Huang, F. Hu, B. He and Z. Ye, *Nanoscale*, 2013, **5**, 10461.
20. R. Dhanalakshmi, A. Pandikumar, K. Sujatha and P. Gunasekaran, *Mater. Express*, 2013, **3**, 291.
21. A. Pandikumar, S. Murugesan and R. Ramaraj, *ACS Appl. Mater. Interfaces*, 2010, **2**, 1912.
22. S. S. Shinde, C. H. Bhosale and K. Y. Rajpure, *Catal. Rev.*, 2013, **55**, 79.
23. Z. Zou, C. Xie, S. Zhang, X. Yu, T. Zou and J. Li, *J. Alloys Compd.*, 2013, **581**, 385.
24. B. Jiang, S. Zhang, X. Guo, B. Jin and Y. Tian, *Appl. Surf. Sci.*, 2009, **255**, 5975.
25. S. Prabhu, T. Viswanathan, K. Jothivenkatachalam and K. Jegannathan, *Indian J. Mater. Sci.*, 2014, **2014**, 10.
26. A. Primo, T. Marino, A. Corma, R. Molinari and H. García, *J. Am. Chem. Soc.*, 2011, **133**, 6930.
27. K. Gurumurugan, D. Mangalaraj, S. K. Narayandass, K. Sekar and C. P. G. Vallabhan, *Semicond. Sci. Technol.*, 1994, **9**, 1827.
28. H. Khallaf, C.-T. Chen, L.-B. Chang, O. Lupan, A. Dutta, H. Heinrich, A. Shenouda and L. Chow, *Appl. Surf. Sci.*, 2011, **257**, 9237.
29. D. M. Carballeda-Galicia, R. Castaneda-Pérez, O. Jiménez-Sandoval, S. Jiménez-Sandoval, G. Torres-Delgado and C. I. Zúñiga-Romero, *Thin Solid Films*, 2000, **371**, 105.
30. K. Gurumurugan, D. Mangalaraj, S. K. Narayandass and Y. Nakanishi, *Mater. Lett.*, 1996, **28**, 307.
31. A. A. Tahir, K. C. Molloy, M. Mazhar, G. Kociok-Köhn, M. Hamid and S. Dastgir, *Inorg. Chem.*, 2005, **44**, 9207-9212.
32. P. K. Larsen, R. Cuppens and G. A. C. M. Spierings, *Ferroelectrics*, 1992, **128**, 265.
33. M. Shahid, M. Hamid, M. Mazhar, J. Akhtar, M. Zeller and A. D. Hunter, *Inorg. Chem. Commun.*, 2011, **14**, 288.
34. M. Veith, M. Haas and V. Huch, *Chem. Mater.*, 2004, **17**, 95.
35. N. Nawar and N. Hosny, *Transition Met. Chem.*, 2000, **25**, 1.
36. M. A. Mansoor, M. A. Ehsan, V. McKee, N.-M. Huang, M. Ebadi, Z. Arifin, W. J. Basirun and M. Mazhar, *J. Mater. Chem. A*, 2013, **1**, 5284.
37. W. Asker and A. Wylie, *Aust. J. Chem.*, 1965, **18**, 959.
38. B. P. Sobolev, *The Rare Earth Trifluorides: The high temperature chemistry of the rare earth trifluorides*, Institut d'Estudis Catalans, 2000.

39. V. Grover, R. Shukla, R. Kumari, B. P. Mandal, P. K. Kulriya, S. K. Srivastava, S. Ghosh, A. K. Tyagi and D. K. Avasthi, *Phys. Chem. Chem. Phys.*, 2014, **16**, 27065.
40. K. Ramesh, L. Chen, F. Chen, Y. Liu, Z. Wang and Y.-F. Han, *Catal. Today*, 2008, **131**, 477.
41. M. Guo, J. Lu, Y. Wu, Y. Wang and M. Luo, *Langmuir*, 2011, **27**, 3872.
42. I. Kosacki, T. Suzuki, H. U. Anderson and P. Colomban, *Solid State Ionics*, 2002, **149**, 99.
43. P. Zinin, L. Tatsumi-Petrochilos, L. Bonal, T. Acosta, J. Hammer, S. Gilder and M. Fuller, *Am. Mineral.*, 2011, **96**, 1537.
44. M. Pal, U. Pal, J. M. G. Y. Jiménez and F. Pérez-Rodríguez, *Nanoscale Res. Lett.*, 2012, **7**, 1.
45. A. A. Tahir, M. A. Ehsan, M. Mazhar, K. G. U. Wijayantha, M. Zeller and A. D. Hunter, *Chem. Mater.*, 2010, **22**, 5084.
46. M. J. H.-S. Toivo T. Kotas, *The Chemistry of Metal CVD*, VCH: Weinheim, 1994.
47. A. Koley, C. T. O'Donohue, M. M. Nolan, K. R. McClain, R. O. Bonsu, R. Y. Korotkov, T. Anderson and L. McElwee-White, *Chem. Mater.*, 2015, **27**, 8326.
48. V. Markoulaki I, I. Papadas, I. Kornarakis and G. Armatas, *Nanomater.*, 2015, **5**, 1971.
49. S. Ahmed, M. A. Mansoor, M. Mazhar, T. Sohnell, H. Khaledi, W. J. Basirun, Z. Arifin, S. Abubakar and B. Muhammad, *Dalton Trans.*, 2014, **43**, 8523.
50. R. Verma, S. K. Samdarshi and J. Singh, *J. Phys. Chem. C*, 2015, **119**, 23899.
51. C. Karunakaran and P. Gomathisankar, *ACS Sustainable Chem. Eng.*, 2013, **1**, 1555.
52. S. A. Ansari, M. M. Khan, M. O. Ansari, S. Kalathil, J. Lee and M. H. Cho, *RSC Adv.*, 2014, **4**, 16782.
53. J. van Elp, R. Potze, H. Eskes, R. Berger and G. Sawatzky, *Phys. Rev. B*, 1991, **44**, 1530.
54. N. Yan, Z. Zhu, J. Zhang, Z. Zhao and Q. Liu, *Mater. Res. Bull.*, 2012, **47**, 1869.
55. N. S. Arul, D. Mangalaraj, R. Ramachandran, A. N. Grace and J. I. Han, *J. Mater. Chem. A*, 2015, **3**, 15248.
56. A. Elaziouti, N. Laouedj, A. Bekka and R.-N. Vannier, *J. King Saud University - Science*, 2015, **27**, 120.
57. A. A. Tahir and K. G. U. Wijayantha, *J. Photochem. Photobiol. A: Chemistry*, 2010, **216**, 119.
58. N. C. Strandwitz, D. J. Comstock, R. L. Grimm, A. C. Nichols-Nielander, J. Elam and N. S. Lewis, *J. Phys. Chem. C*, 2013, **117**, 4931.
59. M. A. Mansoor, M. Mazhar, V. McKee and Z. Arifin, *Polyhedron*, 2014, **75**, 135.

Table of content

Low temperature (475 °C) fabrication of CeO₂-MnO composite thin films having a band gap of 2.5 eV by AACVD.

Graphic

